Scientific paper

Inversion of global tide gauge data for present-day ice load changes

Hans-Peter Plag[1] and Hans-Ulrich Jüttner[2]

[1] *Norwegian Mapping Authority, Kartverksveien 21, N-3511 Hønefoss, Norway*
[2] *Institute for Geophysics, University Kiel, Kiel, Germany*

Abstract: Trends in relative sea level as recorded by the large number of coastal tide gauges are used to derive new constraints on trends in the Antarctic and Greenland ice sheets on century time scales. Based on the sea-level equation, which describes the spatial pattern of sea-level changes due to changes in the ice masses, for each ice sheet the finger-print function for a constant trend is derived. These finger-print functions are used to determined the best-fit trends from the tide gauge trends.

A fit to all tide gauge trends excluding only those with unreasonably large values indicates negative rates of approximately −50 mm/yr for the Antarctic ice sheet and −50 to −100 mm/yr for the Greenland ice sheet, with the latter strongly depending on the model used to predict the post-glacial signal. However, excluding tide gauge trends from lower latitudes, the fit results in positive trends for both the Antarctic and Greenland ice sheets. This high sensitivity of the inversion to a zonal selection of tide gauges indicates that the tide gauge trends may be contaminated by a latitude-dependent steric effect due to zonal warming of the ocean water.

1. Introduction

The 1995 IPCC assessment (Houghton *et al.*, 1996) focuses on the uncertainties in our knowledge of global change, and with respect to changes in the cryosphere, Warrick *et al.* (1996) emphasize the large uncertainties in the contribution of the ice sheets to sea level changes (see Table 1). These uncertainties are due to several circumstances. Firstly, the accuracy of satellite altimetry over ice is still not sufficient to determine the change in the surface height of the large ice sheets, particularly over areas with steep topography, on a level required to reduce the uncertainties. Secondly, the response of glaciers and ice sheets to climate change happens on long time scales of possibly up to several centuries. Therefore, the input forcing function (*i.e.* climate variability) is not well enough determined both in space and time to drive ice mass balance models satisfactorily. Moreover, ground observations to constrain the ice models are scarce compared to the extent of the ice sheets and cover only in a few cases time periods of decades and centuries. Thirdly, observations of global ocean mass (GOM) changes would help to constrain the overall mass balance of the cryosphere. However, the determination of GOM changes from relative sea level (RSL) observations at tide gauges are hampered by the temporal and spatial structure of the global data set as well as the complex physical relation between GOM and RSL. Moreover, global ocean volume (GOV) changes can be due to both mass changes and temperature changes

Table 1.   Uncertainties in factors contributing to global sea-level change. The numbers are according
           to Warrick et al. (1996).

Source	Estimated rate of sea level change (mm/yr)
Steric effects	0.2 to 0.7
Antarctica	−1.4 to 1.4
Greenland	−0.4 to 0.4
Glaciers	0.2 to 0.5
Continental ground waters	−0.5 to 0.7

(steric volume changes), and the separation is not easily achieved. In addition, RSL is affected by other factors than GOV changes constituting a high "noise" level in RSL. Fourthly, the determination of GOM changes from satellite altimetry is still not possible with sufficient accuracy due to the short interval of observation and problems in the separation of steric (volume) and mass effects.

In this unsatisfactory situation, additional observational evidence or methodological approaches that can help to constrain changes in the cryosphere should be sought. Here we attempt a new exploitation of the global tide gauge data set for constraints on changes in the cryosphere. Based on the physical relation between ice load and GOM changes and RSL, an inversion of the local trends at the tide gauges for trends in the large ice sheets is carried out.

GOM and GOV constitute two quantities characterising the ocean as a reservoir in the global hydrological cycle. Changes in GOM and GOV are directly related to changes in the hydrological cycle and therefore to climate change. On climatological time scales, the cryosphere has the greatest potential to contribute to changes in GOM, a fact which has been documented very clearly during the ice ages. GOV changes (for constant mass) are due to density changes resulting primarily from heat exchange with the atmosphere. It is important to note that GOM and GOV are absolute numbers.

Sea level, on the other hand, always is a relative quantity given with respect to a coordinate system (e.g. a geocentric coordinate system) or a reference plane (e.g. a geoid model or the reference ellipsoid). Sea level describes how the GOM is distributed in a given topography of the Earth surface. This distribution depends on many different factors, such as the Earth's topography, the (time-variable) geoid, changes of the Earth's rotation, atmospheric circulation, heat and salinity distribution in the ocean, ocean circulation, present and past mass movements in the Earth system, the viscoelastic properties of the Earth's interior, sedimentation, and even anthropogenic subsidence due to groundwater, gas, or oil extraction.

Whenever mass is exchanged between the ocean and any other reservoirs, sea level is changed in a complex way. A mass movement from or to the ocean changes all geocentric and relative positions of the planes relevant to sea level, i.e., ocean bottom, the reference ellipsoid, the geoid and the sea surface.

Nevertheless, in most studies of the past twenty years, observations of coastal RSL obtained with tide gauges have been used to estimate a global sea level rise (GSLR) and to convert this into a GOV changes without taking into account the complex relation between local RSL and GOV (for a review, see Warrick et al., 1996). Based on a unique data set of monthly mean sea levels derived from tide-gauge observations, the global trend

has been estimated to be of the order of 1–2.5 mm/yr. This relatively wide range mainly is due to the selection criteria used by the different researchers to select subsets of tide gauges. In earlier studies, simple arithmetic averages of selected subsets of tide gauges were considered to be representative for the GSLR (*e.g.* Barnett, 1984). Gornitz and Lebedeff (1987) used geological data to separate the present-day trend from past geological contributions, while Peltier and Tushingham (1989) corrected for the present-day RSL changes due to the last glaciation on the basis of geophysical models. One major conclusion from these studies concerns the length of the records required to determine a reliable local trend at any given tide gauge: due to large decadal to inter-decadal variability of coastal sea level, a record length of the order of 50 years appears to be necessary to determine local trends with a precision of 0.5 mm/yr. Recently, Douglas (1991, 1992, 1995) selected a small number of tide gauges with long records in areas considered as tectonically stable and corrected the local trends for the post-glacial contribution. He then used the consistency of the local trends at these tide gauges as indication that they represent the GSLR.

A few authors have criticised the approach used to determine a GSLR from tide gauges (Pirazzoli, 1989, 1993; Gröger and Plag, 1993; Plag, 1993). Plag (1993) even claimed that it is not possible to determine a global sea level change from tide gauges due to their poor spatial sampling. Previous studies used the complex relation between GOM changes and RSL changes only for the correction of the postglacial rebound effect due to the last deglaciation. Utilising the full physical relationship between sea level and GOM changes, the tide gauges could well be sufficient to constrain the mass movement having contributed to the observed trends in local RSL. This is attempted here for the first time.

It is well known that the disintegration of the last great ice sheets produced a distinct spatial pattern, a finger-print, in RSL, with rather different temporal characteristics of the RSL in the near-intermediate and far field of the load changes (see, *e.g.*, Quinlan and Beaumont, 1982; Lambeck, 1993). The elastic response of the Earth to present-day changes in the cryosphere can be expected to produce a similar finger-print, which should be present in the tide gauge data. Based on these finger-prints, tide gauge trends, in principle, can be inverted for ice load changes.

In the next section, we will first present the well-known equation for RSL changes due to surface mass changes on a visco-elastic and self-gravitating Earth, and specialise this sea-level equation for century scale processes on a simplified Earth model. Based on this equation, in Section 3, we will introduce the concept of finger-prints, which describe sea-level changes due to changes in the thickness of large ice sheets. The finger-print functions are then used to define a model function, which describes local RSL trends as a super-position of the finger-print functions of several ice sheets. In Section 4, we will discuss the RSL databases and the quality of the RSL trends, that can be derived from this database. Results for ice thickness changes of the Antarctic and Greenland ice sheets determined in a fit of the model function to the RSL trends are presented in Section 5 and the sensitivity of the ice thickness trends on different selection criteria for tide gauges are considered. Finally, an interpretation of the results is attempted in Section 6.

2. Sea level changes due to surface mass movements

A linar description of the relation between changes in the Earth's ice cover and RSL

was first given by Farrell and Clark (1976) as the hydrostatic relative sea level equation on a viscoelastic Earth, which we write here as

$$\xi(\vartheta,\lambda,t) = c(t) + \int^{t} \int_{0}^{\prime} \int_{0}^{2\pi} G(\vartheta,\lambda,\vartheta',\lambda',t-t')$$

$$\frac{\mathrm{d}}{\mathrm{d}t'}\{\rho_{w}O(\vartheta',\lambda',t')\xi(\vartheta',\lambda,t') + \rho_{i}[1-O(\vartheta',\lambda',t')]\eta(\vartheta',\lambda',t')\}\sin\vartheta'\,\mathrm{d}\lambda'\,\mathrm{d}\vartheta'\,\mathrm{d}t'. \quad (1)$$

Here, ξ is the sea level change relative to the (deformable) solid Earth surface. G is the Green's function for sea level defined below, O is the ocean function, defined as

$$O(\vartheta,\lambda,t) := \begin{cases} 1 \text{ on oceans} \\ 0 \text{ on continents} \end{cases}, \quad (2)$$

and η the cumulated ice load change due to mass added or removed from land. $c(t)$ is determined such that mass is conserved, i.e.

$$\langle \xi(t) \rangle_{0} = -\frac{\rho_{i}\langle \eta(t) \rangle_{E}}{\rho_{w}\langle O(t) \rangle_{E}} \quad (=\text{eustatic change}), \quad (3)$$

where $\langle \cdot \rangle_{E}$ denotes an average over the Earth's surface, e.g.

$$\langle \eta \rangle_{E} = \frac{1}{4\pi} \int_{0}^{\pi} \int_{0}^{2\pi} \eta(\vartheta,\lambda)\sin\vartheta\,\mathrm{d}\lambda\,\mathrm{d}\vartheta, \quad (4)$$

and $\langle \cdot \rangle_{0}$ indicates an average over the oceans, e.g.

$$\langle \xi \rangle_{0} = \frac{\langle O\xi \rangle_{E}}{\langle O \rangle_{E}} = \frac{\int_{0}^{\pi} \int_{0}^{2\pi} O(\vartheta,\lambda)\xi(\vartheta,\lambda)\sin\vartheta\,\mathrm{d}\lambda\,\mathrm{d}\vartheta}{\int_{0}^{\pi} \int_{0}^{2\pi} O(\vartheta,\lambda)\sin\vartheta\,\mathrm{d}\lambda\,\mathrm{d}\vartheta}. \quad (5)$$

Strictly speaking, ξ as defined by eq. (1) is a continuation of RSL on the continents as well and the true RSL has to be defined as

$$\hat{\xi} := O\xi. \quad (6)$$

However, the function ξ has the decisive advantage over $\hat{\xi}$ of being continuous at the coastlines. Since most of the sea-level stations are located at coastlines of continents where $\hat{\xi}$ has discontinuities, approximations to $\hat{\xi}$ must fail to give correct values of RSL in these stations. Approximations to ξ, on the other hand, have no problem with these locations.

Equation (1) does not consider any dynamic effects in the ocean due to the mass movements, i.e., it is assumed that all processes are slow enough for the ocean to respond hydrostatically to the changes. Dickman (1997) estimated dynamic effects due to seasonal melting and growth of the Antarctic ice sheet and found these effects at annual time scales to be of the order of a few mm. Thus, for considerations of century trends in the ice sheets, dynamic effects safely can be neglected.

Based on a Maxwell rheology and a simple Earth model, Farrell and Clack (1976) showed that the viscous contribution 1000 years after a significant mass change is still of the order of 10% of the initial combined instantaneous effect of elastic deformation and gravitation. Moreover, the spatial pattern of the sea-level changes is not significantly changed by the viscous contribution. Gasperini et al. (1986) considered present-day cryogenic forcing of perturbations in the Earth's rotation and found that a transient

rheology may be important in the modelling of the response due to such a forcing on time scales of centuries. However, for an initial first order study, we assume that the most important contribution to the sea-level change pattern is due to the instantaneous elastic response. We will discuss the validity of this assumption below together with the results of the inversion.

As discussed in Farrell (1972) and Peltier (1974) for the elastic and viscoelastic case, respectively, the Green's function G can be computed for a given spherically symmetric elastic (viscoelastic) isotropic Earth model (SNRE(V)I) model. Thus, for a known load history, the sea-level variations can be computed for such a simplified Earth model.

In specialising eq. (1) for century-scale sea-level changes on an elastic Earth, we assume that changes in the load history are linear trends everywhere, therefore, at any given tide gauge, we expect a linear trend.

For a SNREI Earth, the Green's function for sea level is deduced by Farrell and Clack (1976) to be

$$G(\vartheta,\lambda,\vartheta',\lambda')=\frac{3}{4\pi\rho_o}\sum_{n=0}(1+k_n-h_n)P_n(\cos\theta)$$

$$=\frac{3}{4\pi\rho_o}\sum_{n=0}(1+k_n-h_n)P_n(\sin\vartheta\sin\vartheta'\cos(\lambda-\lambda')+\cos\vartheta\cos\vartheta'), \qquad (7)$$

where ϑ is the angle between the observer and the load, and k_n and h_n are the elastic load Love numbers for the incremental gravitational potential due to the elastic deformation of the Earth and the vertical crustal displacement, respectively, and ρ_o ist the mean density of the Earth. Thus, the sea-level change with respect to a benchmark fixed on the crust is given as the sum of the vertical movement described by h_n, and the geoid change given by $1+k_n$. Here, the one accounts for the Newtonian potential of the mass being moved on the Earth's surface and k_n accounts for the deformations of the Earth's interior.

With this Green's function, we may simplify eq. (1) and write it as

$$\xi(\vartheta,\lambda)=\frac{1}{g_o}\left(\phi(\vartheta,\lambda)-\langle\phi\rangle_o\right)-\left(H(\vartheta,\lambda)-\langle H\rangle_o\right)-\frac{\rho_i\langle\eta\rangle_E}{\rho_w\langle O\rangle_E}. \qquad (8)$$

Here, H is the radial displacement of the Earth's surface and ϕ the incremental gravitational potential generated by the total ice and water load on the Earth and by the accompanying deformation of the Earth. Both, H and ϕ depend on the global distribution of ξ. It is worthwhile to note that ξ is the quantity observed at a given tide gauge but is not equivalent to the geocentric sea-level as measured by satellite altimetry.

Passing over to harmonic developments, e.g.

$$\xi(\vartheta,\lambda)=\sum_{n=0}\sum_{m=-n}^{n}\xi_{nm}Y_{nm}(\vartheta,\lambda), \qquad (9)$$

results into

$$H_{nm}=\frac{3}{\rho_o}\frac{h_n}{2n+1}\left(\rho_w\hat{\xi}_{nm}+\rho_i\eta_{nm}\right), \qquad (10)$$

$$\phi_{nm}=\frac{3g_o}{\rho_o}\frac{1+k_n}{2n+1}\left(\rho_w\hat{\xi}_{nm}+\rho_i\eta_{nm}\right), \qquad (11)$$

and

$$\hat{\xi}_{nm}=(-1)^m\sum_{p=0}^{\infty}\sum_{q=0}^{\infty}\sum_{j=-p}^{p}\sqrt{\frac{(2n+1)(2p+1)(2q+1)}{4\pi}}\begin{pmatrix}n & p & q\\ 0 & 0 & 0\end{pmatrix}\begin{pmatrix}n & p & q\\ -m & j & m-j\end{pmatrix}O_{qm-j}\xi_{pj}, \qquad (12)$$

$$\langle H\rangle_o=\frac{1}{4\pi\langle O\rangle_E}\sum_{n=0}^{\infty}\sum_{m=-n}^{n}(-1)^m H_{nm}O_{n-m}, \qquad (13)$$

$$\langle \phi\rangle_o=\frac{1}{4\pi\langle O\rangle_E}\sum_{n=0}^{\infty}\sum_{m=-n}^{n}(-1)^m \phi_{nm}O_{n-m}, \qquad (14)$$

where g_o is the gravitational acceleration at the surface of the Earth and the symbols $\begin{pmatrix}n_1 & n_2 & n_3\\ m_1 & m_2 & m_3\end{pmatrix}$ denote Wigner 3-j symbols known from the theory of coupling of angular momentums in quantum mechanics (see *e.g.* Edmonds, 1957). Thereby, the sea level eq. (8) may be rewritten in terms of spherical harmonic coefficients as

$$\xi_{nm}=3\frac{1+k_n-h_n}{2n+1}\Bigg\{\frac{\rho_1}{\rho_o}\eta_{nm}$$

$$+(-1)^m\frac{\rho_w}{\rho_o}\sum_{p=0}^{\infty}\sum_{q=0}^{\infty}\sum_{j=-p}^{p}\sqrt{\frac{(2n+1)(2p+1)(2q+1)}{4\pi}}\begin{pmatrix}n & p & q\\ 0 & 0 & 0\end{pmatrix}\begin{pmatrix}n & p & q\\ -m & j & m-j\end{pmatrix}O_{qm-j}\xi_{pj}\Bigg\}$$

$$-\Bigg\{\frac{3}{O_{00}}\frac{\rho_w}{\rho_o}\sum_{p=0}^{\infty}\sum_{q=0}^{\infty}\sum_{r=0}^{\infty}\sum_{j=-p}^{p}\sum_{i=-q}^{q}\frac{1+k_p-h_p}{2p+1}\sqrt{\frac{(2p+1)(2q+1)(2r+1)}{4\pi}}\begin{pmatrix}p & q & r\\ 0 & 0 & 0\end{pmatrix}\begin{pmatrix}p & q & r\\ -j & i & j-i\end{pmatrix}O_{p-j}O_{ri-j}\xi_{qi}$$

$$+\frac{3}{O_{00}}\frac{\rho_1}{\rho_o}\sum_{p=0}^{\infty}\sum_{j=-p}^{p}(-1)^j\frac{1+k_p-h_p}{2p+1}O_{p-j}\eta_{pj}+\sqrt{4\pi}\frac{\rho_1}{\rho_w}\frac{\eta_{00}}{O_{00}}\Bigg\}\delta_{n0}\delta_{m0}. \qquad (15)$$

Equations (9) and (15) are linear. Therefore, taking time derivatives, it is seen that formally the same equations are satisfied by sea-level and ice-load trends. Thus, eq. (15) in principle can be used to invert local RSL trends determined at a sufficient number of tide gauges for trends in the ice sheets.

3. The concept of finger-print function

We will, for the time being, assume that we are able to determine reliable RSL trends at a sufficient number of tide gauges and correct these trends for all other effects not due to present-day changes in the ice loads. Below, we use $\alpha=\dot{\xi}$ and $\beta=\dot{\eta}$ to denote the linear trends in sea-level and the ice sheets, respectively. α_i denotes the trend in RSL at the i-th tide gauge.

There are two main approaches for the inversion of the available sea-level observations for ice-load trends. The first one is to fit spherical harmonic coefficients α_{nm} up to a maximal degree n_o by a least squares method to station data $\alpha_i=\alpha(\vartheta_i,\lambda_i)$ using eq. (9). Then, eq. (15) is inverted for the harmonic coefficients β_{pj} up to the same maximal degree n_o. This yields the spatial distribution of the linear trend in the ice-load. However, the solution is subject to major uncertainties due to the spatially incomplete distribution of tide gauges with most sites located along the coasts of the northern hemisphere. Moreover, the number of unknowns β_{pj} is large and may exceed the number of tide gauges with reliable trends for any reasonable value of n_o.

Therefore, the second approach is to reduce the number of unknowns through parametrising the ice-load trends. Then eqs. (9) and (15) can be used together to determine

the parameters of the ice load by a least squares method. If there are only a few free parameters to adjust, this avoids much of the uncertainties of the former solution. However, the quality of this solution depends strongly on the selected ice-load model. If the ice-load model is incorrect, the solution based on it might be misleading.

Below we will explore the second approach. For that, we assume a constant trend in ice cover over each of the major ice sheets. This assumption is not justified by the known processes on ice sheets and glaciers, where large spatial variations in ablation or accretion are observed. However, the spatial resolution of the tide gauge data set is not good enough to resolve small-scale variability. Nevertheless, we should be able to determine whether the Greenland and Antarctic ice sheets are on average increasing or decreasing. Therefore, the assumption can be justified as a first step.

For linear changes on each of the major ice sheets we can computed the finger-print in the RSL trends for a unit trend. Let $g^{(k)}$ be the characteristic function of the k-th glacier, defined as

$$g^{(k)}(\vartheta,\lambda)=\begin{cases} 1 & \text{on the glacier number } k \\ 0 & \text{otherwise} \end{cases} \tag{16}$$

with harmonic development

$$g^{(k)}(\vartheta,\lambda)=\sum_{n=0}^{\infty}\sum_{m=-n}^{n} g_{nm}^{(k)} Y_{nm}(\vartheta,\lambda). \tag{17}$$

Assuming that the sea-level eq. (8) has a unique solution for η replaced with any of the characteristic functions (16), these solutions shall be called the *finger-print functions* of the k-th glacier and be denoted $f^{(k)}(\vartheta,\lambda)$. Then, the corresponding solutions of eq. (15) yield the harmonic coefficients $f_{nm}^{(k)}$ of these finger-print functions, i.e.

$$
\begin{aligned}
f_{nm}^{(k)}=3\,\frac{1+k_n-h_n}{2n+1}\Bigg\{ &\frac{\rho_1}{\rho_o}g_{nm}^{(k)} \\
&+(-1)^{m}\frac{\rho_w}{\rho_o}\sum_{p=0}^{\infty}\sum_{q=0}^{\infty}\sum_{j=-p}^{p}\sqrt{\frac{(2n+1)(2p+1)(2q+1)}{4\pi}}\begin{pmatrix} n & p & q \\ 0 & 0 & 0 \end{pmatrix}\begin{pmatrix} n & p & q \\ -m & j & m-j \end{pmatrix}O_{qm-j}f_{pj}^{(k)}\Bigg\} \\
-\Bigg\{&\frac{3}{O_{00}}\frac{\rho_w}{\rho_o}\sum_{p=0}^{\infty}\sum_{q=0}^{\infty}\sum_{r=0}^{\infty}\sum_{j=-p}^{p}\sum_{pi=-q}^{q}\frac{1+k_p-h_p}{2p+1}\sqrt{\frac{(2p+1)(2q+1)(2r+1)}{4\pi}}\begin{pmatrix} p & q & r \\ 0 & 0 & 0 \end{pmatrix}\begin{pmatrix} p & q & r \\ -j & i & j-i \end{pmatrix}O_{p\,i}O_{rj-i}f_{qi}^{(k)} \\
&+\frac{3}{O_{00}}\frac{\rho_1}{\rho_o}\sum_{p=0}^{\infty}\sum_{j=-p}^{p}(-1)^{j}\frac{1+k_p-h_p}{2p+1}O_{p-j}g_{pj}^{(k)}+\sqrt{4\pi}\frac{\rho_1}{\rho_w}\frac{g_{00}^{(k)}}{O_{00}}\Bigg\}\delta_{n0}\delta_{m0}.
\end{aligned} \tag{18}
$$

With these finger-prints, the trend at tide gauge i may be approximated as

$$\alpha_i=\sum_{k=1}^{K}\beta_k f^{(k)}(\vartheta_i,\lambda_i)+c, \tag{19}$$

where β_k is the (unknown) constant trend for the k-th ice mass, $f^{(k)}$ the unit finger-print function for this ice mass, K the number of ice masses considered, ϑ_i and λ_i are the geographical coordinates of the tide gauge, and c is a constant included to account for a global sea level change not being due to ice load changes. Finally, the β_k can be estimated in a least squares fit of eq. (19) to the trends determined from the tide gauges.

For practical calculations the eqs. (15) and (18) have to be truncated at a maximal degree n_o. This results in the matrix equation

$$\sum_{p=0}^{n_o}\sum_{j=-p}^{p} A_{nm,pj}^{(n_s)}\xi_{pj}=\sum_{p=0}^{n_s}\sum_{j=-p}^{p} B_{nm,pj}^{(n_s)}\eta_{pj}, \tag{20}$$

with matrix elements

$$A^{(n_s)}_{nm,pj} := \delta_{np}\delta_{mj}$$

$$+\frac{3}{O_{00}}\frac{\rho_w}{\rho_o}\sum_{q=0}^{n_s}\sum_{r=0}^{n_s}\sum_{i=-q}^{q}\frac{1+k_q-h_q}{2q+1}\sqrt{\frac{(2p+1)(2q+1)(2r+1)}{4\pi}}\begin{pmatrix}p & q & r\\0 & 0 & 0\end{pmatrix}\begin{pmatrix}p & q & r\\j & -i & i-j\end{pmatrix}O_{q-i}O_{r,i-j}\delta_{n0}\delta_{m0}$$

$$-3(-1)^m\frac{\rho_w}{\rho_o}\frac{1+k_n-h_n}{2n+1}\sum_{q=0}^{n}\sqrt{\frac{(2n+1)(2p+1)(2q+1)}{4\pi}}\begin{pmatrix}n & p & q\\0 & 0 & 0\end{pmatrix}\begin{pmatrix}n & p & q\\-m & j & m-j\end{pmatrix}O_{qm-j}, \quad (21)$$

and

$$B^{(n_s)}_{nm,pj} := 3\frac{1+k_n-h_n}{2n+1}\frac{\rho_1}{\rho_o}\delta_{np}\delta_{mj}-\left\{(-1)^j\frac{3}{O_{00}}\frac{\rho_1}{\rho_o}\frac{1+k_p-h_p}{2p+1}O_{p-i}\right.$$

$$\left.+\frac{\sqrt{4\pi}}{O_{00}}\frac{\rho_1}{\rho_w}\delta_{p0}\delta_{j0}\right\}\delta_{n0}\delta_{m0}. \quad (22)$$

With matrix

$$S^{(n_s)} := A^{(n_s)^{-1}}B^{(n_s)}, \quad (23)$$

the solution of the matrix eq. (20) reads $\xi_{nm}=\sum_{p=0}^{n_s}\sum_{j=-p}^{p}S^{(n_s)}_{nm,pj}\eta_{pj}$.

By this, approximations $f^{(k,n_s)}$ to the footprint functions $f^{(k)}$ are defined as

$$f^{(k,n_s)}_{nm} := \sum_{p=0}^{n_s}\sum_{j=-p}^{p}S^{(n_s)}_{nm,pj}g^{(k)}_{pj}, \quad (24)$$

$$f^{(k,n_s)}(\vartheta,\lambda) := \sum_{n=0}^{n}\sum_{m=-n}^{n}f^{(k,n_s)}_{nm}Y_{nm}(\vartheta,\lambda). \quad (25)$$

It has to be shown that these approximations actually converge in a certain sense to the true footprint functions $f^{(k)}$. Furthermore, an n_0 has to be found, for which the approximations are sufficiently close to the footprint functions $f^{(k)}$ for all glaciers.

No mathematically rigorous proof of convergence of the approximation to the footprint functions is attempted here. Instead, in Fig. 1, the trends predicted at individual tide gauges are given as function of the cut-off degree n_0. At all tide gauges, the trend predictions are stable for $n_0 > 40$ and no significant variations occur at higher values of n_0. It is interesting to note here that the trends at tide gauges in the far field do not show large variations from gauge to gauge, while at gauges closer to the ice loads large variations in the predicted trends are found.

In Fig. 2 the boundaries of the ice sheets are given for the cut-off degree of $n_0 = 69$. This approximation represents the boundaries of the ice sheets already to a great detail.

The finger-prints of the Antarctic and Greenland ice sheets are given in Fig. 3. For a unit increase of the Antarctic ice sheet, sea level will basically tilt from South to North with very little dependency on longitude, while a similar increase of the Greenland ice sheet will result in an opposite tilt from North to South but additionally a dependency on longitude for high northern latitudes.

The finger-prints of Antarctic and Greenland to a large extent are anti-correlated. This may cause problems in separating the effect of the two ice sheets if the overall trends have opposite sign. Furthermore, the success of a fit of the model function to the tide gauge trends depends also on the geographical distribution of the tide gauges. This will be discussed in the next section.
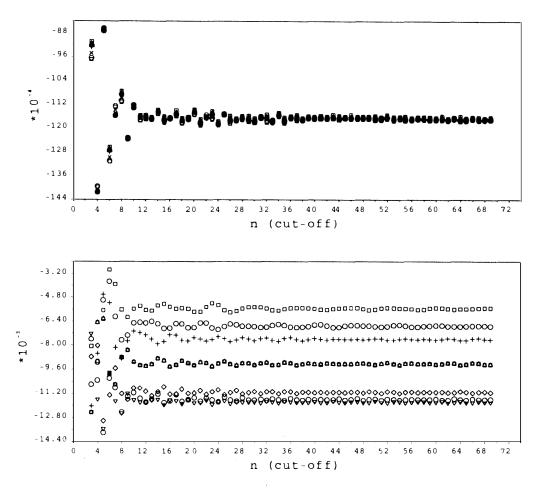
Fig. 1. Trends predicted by equally weighted finger-prints of the Antarctic, Greenland, and Iceland ice sheets as function of the cut-off degree n_o. Upper diagram: Stations from the coast around Great Britain, lower: from New Zealand. Each symbol represents an individual tide gauge.

4. Determination of RSL trends at tide gauges

The global tide gauge data set provided by the PSMSL (Spencer and Woodworth, 1993) contains more than 1700 records of monthly mean sea levels. These time series are of variable quality and length. The PSMSL separates the total data set into a so-called Metric data set and a Reviced-Local-Reference data set, with the latter one comprising all the records with a well-documented history of the tide-gauge benchmark. For trend determinations, only records in the RLR subset can be used. In this data set, there are 988 records with at least five years of data, with the longest of them covering a span of nearly 200 years.

In Fig. 4 we show the trends as determined from the RLR tide gauges. All trends up to ± 10 mm/yr are displayed. The figure reveals a large scatter of the local trends, which partly can be explained by known tectonic movements and partly by postglacial rebound. To improve the quality of the attempted fit of eq. (19), we have to use as many trend values as possible. Therefore, it is necessary to account for as many disturbing influences as
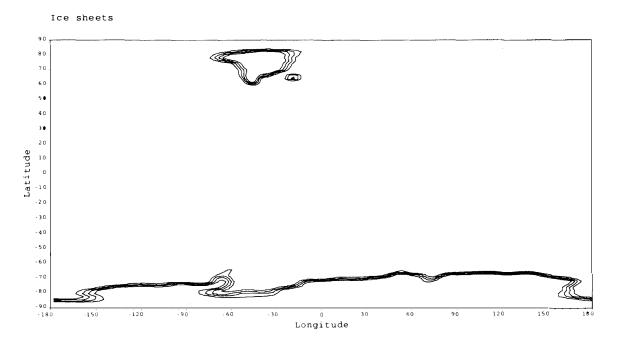
Ice sheets

Fig. 2.   Approximation of the ice sheet functions to degree 69. The nominal value inside and outside
the ice sheets is 1 and 0, respectively. The approximation does not deviate from these values
more than 0.02 except at the boundaries, which have a steep slope. Isolines are from 0 to
1 with step 0.2.

possible.

Basically, the local trends determined from tide gauges are significantly affected by (1)
tectonic movements, (2) postglacial rebound, and (3) decadal to interdecadal variability. We
will discuss these effects one by one.

(1) Large parts of the ocean's coasts are in deformation areas associated with plate
tectonics (see, e.g. Fig. 6 in Stein, 1993). In most of these regions, the tectonically caused
vertical crustal movements are dominated by short spatial scales of the order of 30 to 100
km (see e.g. Emery and Aubrey, 1991). Thus, the ice mass finger-print is distinctively
different from the tectonical signal in sea level and a contamination of the β_k due to
tectonic motion should be small. With respect to the long-wavelength ice signal, the
tectonical signal can be considered as noise. Moreover, in many geographical regions the
vertical crustal motion is of the order of $\pm$ 1 mm/yr and thus smaller than the expected local
signal due to ice mass changes. Therefore, we have not taken any measure to decontaminate
the tide gauge trends for tectonical vertical crustal motion.

(2) The present-day postglacial signal (PGS) in sea level may be highly correlated with
the finger-print of present-day changes in ice sheets. Fortunately, elaborated models exist for
the PGS and these models can be used to decontaminate the tide gauge trends for the PGS.
However, inter-model differences are still considerable. Therefore, we have used a suite of
models in the determination of the ice sheet trends. Moreover, a scale factor was introduced
for the PGS in order to allow for uncertainties in the global amplitude of the PGS. Thus,
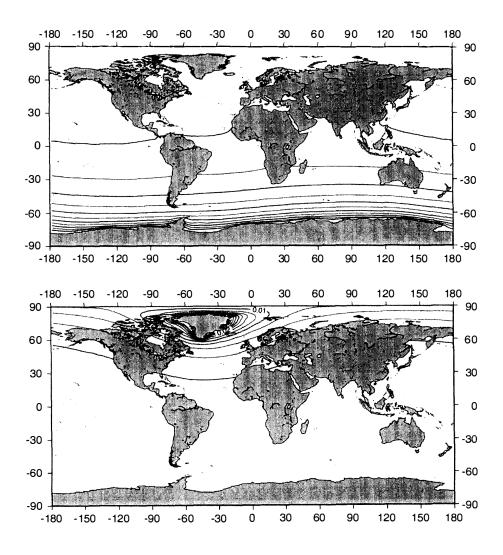eq. (19) is modified to

Fig. 3. RSL finger print of a uniform ice load change across the complete Antarctic (upper diagram) and Greenland (lower diagram) ice sheets. For Antarctica, isolines are from − 0.01 to 0.045 with step − 0.005. Spacing of thick lines is 0.01 and zero line is the third line from top. For Greenland, isoline are from 0. to 0.0275 with step 0.0025. Spacing of thick lines is 0.01 and zero line is the first line from bottom.

$$\alpha_i = \sum_{k=1}^{K} \beta_k f^{(k)}(\vartheta_i, \lambda_i) + \gamma p_i + c, \tag{26}$$

where p_i is the PGS at the tide gauge i and γ the (unknown) scale factor for a given PGS model. It should be mentioned here, however, that since the PGS is closely correlated with the present-day changes, any errors in the PGS will bias the estimates of the present-day changes.

(3) Interannual to multidecadal variations in RSL are mainly due to similar variations in atmospheric and oceanic circulation. In sea-level at costal locations, these variations are of the order of several cm, and thus significantly bias trends determined from records of less than several decades. To determine a local trend from an individual tide gauge with an accuracy of 0.5 mm/yr, records of 60 years are required in most coastal regions (e.g. Zerbini
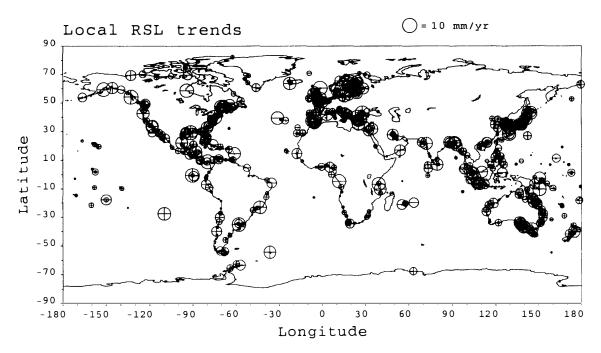
Fig. 4. *Local RSL trends determined from tide gauges. The diameter of the circles at each tide gauge are proportinal to the trend with positive and negative trends indicated by a plus or minus sign, respectively.*

et al., 1996). Both, tide gauge studies (*e.g.* Sturges, 1987; Gröger and Plag, 1993) and satellite altimetry observations (*e.g.* Nerem *et al.*, 1997) have shown that the interannual to multi-decadal sea level variations are spatially coherent over large regions. Therefore, based on a high-quality long record in a given region, shorter records can be decontaminated for the interannual to multidecadal variability (Sjöberg, 1987; Plag, 1988). For that, time series of the monthly differences between the a given shorter record and the base record are computed. These differences are nearly free of the interannual to multidecadal variability. The trend of these differences plus the long-term trend at the base station thus is a decontaminated long-term trend at the station with the shorter record.

In the present study, only the local RSL trends are used without any corrections for interannual to multidecadal variability.

5. Antarctic and Greenland ice thickness changes

The anti-correlation of the Greenland and Antarctic finger-prints in large geographical regions may cause problems if the changes of these two ice sheets have opposite signs. However, taking into account the position of the available tide gauges, the predicted trends at a considerable number of tide gauges depend on the spatial pattern of either the Antarctic or Greenland ice sheets alone while the other ice sheet only contributes a small constant (Fig. 5). Iceland, on the other hand is too close to Greenland for its finger-print to be separable from the Greenland finger-print.

It can be concluded that particularly the tide gauges in the near to medium field of a given ice sheet will be able to detect the finger-print. Thus, Southern hemisphere gauges will
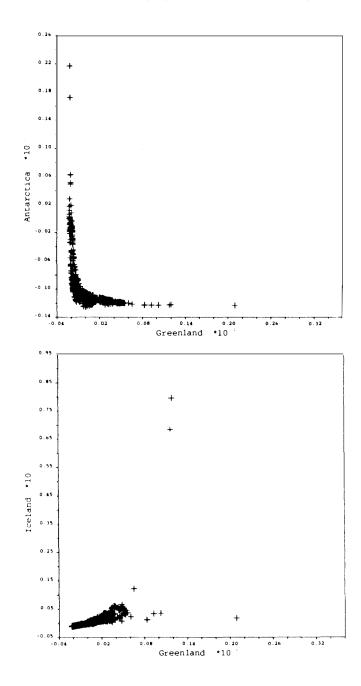
Fig. 5. Comparison of RSL finger prints at tide gauges. Upper diagram: Antarctica versus Greenland; lower diagram Iceland versus Greenland.

constrain the Antarctic ice sheet while Northern hemisphere gauges will do the same for the Greenland ice sheet. Tide gauges at higher latitudes will have a greater effect on the inversion than those at lower latitudes.

Changes in the two large ice sheets having the same sign should result in a finger-print detectable in sea level. Thus, the sum of a unit increase in both ice sheets displays an increase of sea level close to the ice sheets and a decrease at lower latitudes. However, in large geographical regions, a negative change in the Antarctic ice sheet would be correlated

Table 2.   Parametres of the postglacial rebound models from Mitrovica (1996, personal communication).

	Model 1	Model 2
Lithosphere	120 km	120 km
Upper mantle viscosity	1×10^{21} Pas	1×10^{21} Pas
Lower mantle viscosity	2×10^{21} Pas	4.75×10^{21} Pas
Ice model	ICE-3G	ICE-3G

with a positive change for Greenland. Changes with opposite sign for these ice sheets therefore will be difficult to separate.

Based on eq. (26) the finger-print functions have been fitted to the trend data set. In this fit, two different models for the PGS have been used, which only differ in the lower mantle viscosity (Table 2).

In the fit, different constraints have been applied to select subsets of the trend values. These constraints are (1) the latitude ϑ excluding trends from a latitude band centred around the equator; (2) the absolute value of the trend T, excluding those trends larger than a limit; (3) length of record L, excluding trends from records shorter than a lower bound. The results are summarised in Table 3. The resulting trends in the ice sheets are strong dependent on the constraints used to selected subsets of the trend values. Without any constraints, the large trend values dominate the fit. The reduction of standard deviation of the trend data set through this fit is almost zero and solely due to the PGS and the global rise c while the trends for Antarctica and Greenland have opposite sign. Thus, a fingerprint of these ice sheets is not detected. Moreover, if the finger-print for both Greenland and Iceland are included, the results for these two ice sheets are unreasonably large.

Using only tide gauge trends within $| T | < 12$ mm/yr reduces the number of gauges by only 7.7% but this has a strong effect on the fit. Therefore, below we only discuss fits with this constraint applied. If this is the only constraint, then the rates for both Antarctica and Greenland turn out to be negative. For Antarctica, the value does not depend on the PGS model selected and is of the order of -50 mm/yr. On the other hand, for Greenland, PGS model 1 gives decreases of the order of -100 mm/yr while the rates for model 2 are of the order of -50 mm/yr. The scale factor for PGS model 2 is smaller than for model 1, while the constant c representing a global rise in sea level and the reduction of standard deviation of the total fit are larger for model 2.

If the length of the tide gauge record is used as additional constraint with $L > 240$ months, then the negative rate for Greenland is rather large (-189 mm/yr) while the rate for Antarctica is much smaller (-22 mm/yr). However, constraining the length of the time series removes a large fraction of the tide gauges at higher latitudes, *i.e.* in the near-field. Therefore, this may not be a reasonable constraint.

Eliminating all trends from tide gauges within $| \vartheta | < 30°$ reduces the number of tide gauges by almost 30%. However, applying this together with the constraint $| T | < 12$ mm/ yr, results in rates of -29 mm/yr and -124 mm/yr for the Antarctic and Greenland ice sheets, respectively. That is, both ice sheets appear to be decreasing.

The combined constraints $| \vartheta | > 50°$ and $| T | < 12$ mm/yr is the only set resulting in large positive rates for both ice sheets. These constraints eliminate all tide gauges in the far

Table 3. Results of the fits of eq. (26) to the tide gauge trends. The model function is denoted by nI, pm, with n number of ice sheets included, and m number of PGS model. Constraints are applied for latitude ϑ, trend T and record length L. N is the number of stations meeting the constraints. All rates are in mm/yr. Rates are for Antarctica (Ant.), Greenland (Green.) and Iceland (Ice.) and the remaining global average c. The scale factor γ for the PGS model is relative. σ_0 and σ_{res} are the standard deviation of the trend values and the residuals with respect to the model fit, respectively. Red. is the reduction in the standard deviation in %.

Model	$\|\vartheta\|$ °	$\|T\|$ mm/yr	L months	N	Ant.	Green. mm/yr	Ice.	γ	c	σ_0 mm/yr	σ_{res}	Red. %
3I, p1				988	−124	580	1600	0.88		11.14	10.93	1.9
3I, p1, c				988	71	−405	1318	0.96	2.11	11.14	10.93	1.9
2I, p1, c				988	88	−258		0.97	2.32	11.14	10.94	1.8
2I, p2, c				988	88	−181		0.91	2.44	11.14	10.92	2.0
2I, p1, c	>30			708	114	−130		1.00	2.24	10.79	10.56	2.1
2I, p1, c	>30	<12		661	−29	−124		0.83	0.75	3.80	3.34	12.1
2I, p1, c	>30		>240	410	35	−127		0.84	1.33	3.80	3.25	14.4
2I, p1, c	>30	<12	>240	404	12	−154		0.81	1.16	3.02	2.31	23.5
2I, p1, c	>50	<12		216	86	340		0.88	0.36	4.02	3.00	25.4
2I, p1, c			>240	529	1	−214		0.83	1.26	4.09	3.60	12.0
2I, p1, c		<20	>240	526	−4	−191		0.83	1.13	3.40	2.83	16.8
2I, p1, c		<15	>240	524	−12	−195		0.81	1.03	3.23	2.65	18.0
2I, p1, c		<12	>240	521	−22	−189		0.81	0.95	3.09	2.48	19.7
2I, p1, c		<20		959	−13	−114		0.84	1.04	4.95	4.65	6.1
2I, p1, c		<15		937	−58	−93		0.83	0.48	4.22	3.90	7.6
2I, p1, c		<12		921	−56	−117		0.83	0.51	3.88	3.51	9.5
2I, p2, c		<20		959	−16	−57		0.77	1.10	4.95	4.63	6.5
2I, p2, c		<15		937	−59	−31		0.77	0.57	4.22	3.86	8.5
2I, p2, c		<12		921	−57	−52		0.78	0.61	3.88	3.47	10.6

field. Thus, the near-field gauges appear to be best fitted by a growth of both ice sheets. The global signal represented by c appears to be very small (<0.4 mm/yr). The large dependency of the results on the far-field gauges included or excluded may be due to another latitude-dependent signal in the RSL trends, super-imposed on the ice sheet finger-prints. For example, a latitude-dependent warming of the ocean with relatively large warming at lower latitudes would bias the estimated rates for the ice sheets towards lower values and might even cause negative rates for actually growing ice sheets.

6. Discussion

Reasonably selected subsets of the RSL trends determined from the global tide gauges database indicate negative rates of approximately −50 mm/yr for the Antarctic ice sheet and −50 to −100 mm/yr for the Greenland ice sheet. However, the results depend on the selection criteria. Excluding the tide gauges in the far field of the ice sheets results into positive trends for both ice sheets. This high sensitivity of the estimated rates for the ice sheets to the latitudinal constraint for the selection of tide gauges indicates that the rates of relative sea-level changes determined from tide gauges may be contaminated by another

latitude-dependent factor.

This factor may be a combined effect of steric volume changes and changes in the ocean circulation, which both may have a significant latitude-dependent part. Interdecadal variability in ocean circulation and water temperature induces similar sea level variations, which effect trends in relative sea level determined from time series of up to several decades. Taking into account that many tide gauge records cover the last 30–50 years, a bias of the trends can be expected. However, observational data on ocean circulation and density are sparce (Warrick *et al.*, 1996) and the spacial pattern of steric sea-level changes cannot be determined confidently from these observations.

The geographical distribution of steric sea-level variations can also be determined from ocean circulation or coupled atmosphere-ocean circulation models (*e.g.* Gregory, 1993; Bryan, 1996). However, results still show little similarity between different models and, therefore, have low confidence.

Nevertheless, to improve the inversion of the tide gauge data, models for the steric effect need to be taken into account. For example, output from different advanced global circulation model simulations for the last hundred years could be used to study the sensitivity of the inversion to this factor.

Another potential bias of the estimated rates is due to uncertainties in the models used to compute the pgs. (Huybrechts and Le Meur (1999) modelled the present-day pgs of Antarctica and found that this signal may be significantly larger that the one predicted by the models used here. Therefore, the use of more advanced models for the pgs would be an additional improvement of the fits presented here.

Acknowledgments

References

Barnett, T.P. (1984): The estimation of "global" sea level change: a problem of uniqueness. J. Geophys. Res., **89**, 7980–7988.

Bryan, K. (1996): The steric component of sea level rise associated with enhanced greenhouse warming: a model study. Clim. Dyn., **12**, 545–555.

Dickman, S.R (1997): Detection of hypothetical global warming effects. Ann. Geophys., **15** (Supl. 1), C32.

Douglas, B.C. (1991): Global sea level rise. J. Geophys. Res., **96**, 6981–6992.

Douglas, B.C. (1992): Global sea level acceleration. J. Geophys. Res., **97**, 12699–12706.

Douglas, B.C. (1995): Global sea level change: Determination and interpretation. Rev. Geophys., IUGG suppl., 1425–1432.

Edmonds, A.R. (1957): Angular momentum in quantum mechanics. Princeton, Princeton University Press.

Emery, K.O. and Aubrey, D.G. (1991): Sea Levels, Land Levels, and Tide Gauges. Berlin, Springer.

Farrell, W.E. (1972): Deformation of the Earth by surface loads. Rev. Geophys. Space Phys., **10**, 761–797.

Farrell, W.E. and Clark, J.A. (1976): On postglacial sea level. Geophys. J. R. Astron. Soc., **46**, 647–667.

Gasperini, P., Sabadini, R. and Yuen, D.A. (1986): Excitation of the earth's rotational axis by recent

glacial discharges. Geophys. Res. Lett., **13**, 533–536.

Gornitz, V. and Lebedeff, S. (1987): Global sea level changes during the past century. Sea Level Fluctuations and Coastal Evolution, ed. by D. Nummedal *et al.* Soc. Econ. Palaeontol. Miner., 3–16 (Spec. Publ., Vol. 41).

Gregory, J.M. (1993): Sea level changes under increasing atmospheric CO_2 in a transient coupled ocean-atmosphere gcm experiment. J. Clim., **6**, 2247–2262.

Gröger, M. and Plag, H.-P. (1993): Estimations of a global sea level trend: Limitations from the structure of the PSMSL global sea level data set. Global Planet. Change, **8**, 161–179.

Houghton, J.T., MeiraFilho, L.G., Callander, B.A., Harris, N., Kattenberg, A. and Maskell, K., ed. (1996): Climate Change 1995 — The Science of Climate Change. Cambridge, Cambridge University Press.

Huybrechts, P. and LeMeur, E. (1999): Predicted present-day evolution patterns for ice thickness and bedrock elevation over Greenland and Antarctica. Polar Res., **18**, 299–306.

Lambeck, K. (1993): Glacial rebound of the British Isles -I. Preliminary model results, II. A high-resolution, high precision model. Geophys. J. Int., **115**, 941–990.

Nerem, S.M., Rachlin, K.E. and Beckley, B.D. (1997): Characterization of global mean sea level variations observed by TOPEX/POSEIDON using empirical orthogonal functions. Surv. Geophys., **18**, 293–302.

Peltier, W.R. (1974): The impulse response of a Maxwell Earth. Rev. Geophys. Space Phys., **12**, 649–669.

Peltier, W.R. and Tushingham, A.M. (1989): Global sea level rise and the Greenhouse effect: Might they be connected? Science, **244**, 806–810.

Pirazzoli, P.A. (1989): Present and near-future global sea-level changes. Palaeogeogr., Palaeoclimatol., Palaeoecol., **75**, 241–258.

Pirazzoli, P.A. (1993): Global sea-level changes and their measurement. Global Planet. Change, **8**, 135–148.

Plag, H.-P. (1988): A regional study of Norwegian coastal long-period sea-level variations and their causes with special emphasis on the Pole Tide. Berl. Geowiss. Abhandl. Reihe A, **14**, 1–175.

Plag, H.-P. (1993): The "sea level rise" problem: An assessment of methods and data. Proceedings of the International Coastal Congress, Kiel 1992, Frankfurt, P. Lang Verlag, 714–732.

Quinlan, G. and Beaumont, C. (1982): The deglaciation of Atlantic Canada as reconstructed from the post glacial relative sea-level record. Can. J. Earth Sci., **19**, 2232–2246.

Sjöberg, L.E. (1987): Comparison of some methods of determining land uplift rates from tide gauge data. ZfV, **2**, 69–73.

Spencer, N.E. and Woodworth, P.L. (1993): Data holdings of the Permanent Service for Mean Sea Level, Tech. rep., Permanent Service for Mean Sea Level, Bidston, UK, 81 p.

Stein, S. (1993): Space geodesy and plate motion. Contributions of Space Geodesy in Geodynamics: Crustal Dynamics, ed. by D.E. Smith and D.L. Turcotte. Washington, D.C., Am. Geophys. Union, 5–20 (AGU Geodyn. Ser., Vol. 23).

Sturges, W. (1987): Large-scale coherence of sea level at very low frequencies. J. Phys. Oceanogr., **17**, 2084–2094.

Warrick, R.A., Provost, C.I., Meier, M.F., Oerlemans, J. and Woodworth, P.L. (1996): Changes in sea level. Climate Change 1995—The Science of Climate Change, ed. by J.T. Houghton *et al.* Cambridge, Cambridge University Press, 359–405,

Zerbini, S. and 15 colleagues (1996): Sea level in the Mediterranean: a first step towards separation of crustal movements and absolute sea-level variations. Global Planet. Change, **14**, 1–48.